Jab1 regulates Schwann cell proliferation and axonal sorting through p27

Emanuela Porrello,[1] Cristina Rivellini,[1] Giorgia Dina,[1] Daniela Triolo,[1] Ubaldo Del Carro,[2] Daniela Ungaro,[2] Martina Panattoni,[3] Maria Laura Feltri,[4] Lawrence Wrabetz,[4] Ruggero Pardi,[3] Angelo Quattrini,[1,2] and Stefano Carlo Previtali[1,2]

[1]Institute of Experimental Neurology (INSPE), Division of Neuroscience; [2]Department of Neurology; and [3]Division of Immunology, Transplantation, and Infectious Disease; San Raffaele Scientific Institute, 20132 Milan, Italy
[4]Hunter James Kelly Research Institute, School of Medicine and Biomedical Sciences, University at Buffalo, The State University of New York, Buffalo, NY 14203

Axonal sorting is a crucial event in nerve formation and requires proper Schwann cell proliferation, differentiation, and contact with axons. Any defect in axonal sorting results in dysmyelinating peripheral neuropathies. Evidence from mouse models shows that axonal sorting is regulated by laminin211– and, possibly, neuregulin 1 (Nrg1)–derived signals. However, how these signals are integrated in Schwann cells is largely unknown. We now report that the nuclear Jun activation domain–binding protein 1 (Jab1) may transduce laminin211 signals to regulate Schwann cell number and differentiation during axonal sorting. Mice with inactivation of Jab1 in Schwann cells develop a dysmyelinating neuropathy with axonal sorting defects. Loss of Jab1 increases p27 levels in Schwann cells, which causes defective cell cycle progression and aberrant differentiation. Genetic down-regulation of p27 levels in Jab1-null mice restores Schwann cell number, differentiation, and axonal sorting and rescues the dysmyelinating neuropathy. Thus, Jab1 constitutes a regulatory molecule that integrates laminin211 signals in Schwann cells to govern cell cycle, cell number, and differentiation. Finally, Jab1 may constitute a key molecule in the pathogenesis of dysmyelinating neuropathies.

CORRESPONDENCE
Stefano Carlo Previtali:
previtali.stefano@hsr.it

Abbreviations used: cMAP, compound motor action potential; DRG, dorsal root ganglia; NCV, nerve conduction velocity.

In peripheral nerve development, the transition between bundles of growing axons surrounded by Schwann cell processes to individual axon ensheathment is termed axonal sorting (Sherman and Brophy, 2005). This event relies on extensive and regulated Schwann cell proliferation to match axon–Schwann cell number and coordinated withdrawal from the cell cycle, differentiation, and survival (Martin and Webster, 1973; Jessen and Mirsky, 2005). Furthermore, Schwann cells extend longitudinal and radial processes to sort large caliber axons from bundles, adopt a 1:1 relationship, and myelinate them (Martin and Webster, 1973; Webster et al., 1973; Nodari et al., 2007).

Any defect in the process of axonal sorting results in dysmyelinating neuropathies, such as those associated with merosin-deficient congenital muscular dystrophy type 1A (MDC1A; OMIM #607855) in humans (Shorer et al., 1995) and equivalent disorders in spontaneous dystrophic (*dy2J*) and knockout (*dy3k*) mice (Miyagoe et al., 1997; Guo et al., 2003). All of these neuropathies are caused by mutations of the laminin α2 gene (*LAMA2*), which encodes for the α2 subunit of laminin211 (or merosin), the major component of the Schwann cell basal lamina. A hallmark of *Lama2* neuropathies is impaired axonal sorting that resembles embryonic fascicles (Bradley and Jenkison, 1973; Stirling, 1975; Shorer et al., 1995). In fact, laminin211 affects axonal sorting by regulating Schwann cell proliferation and cytoskeletal remodeling. In the process, the laminin receptors αβ1 integrin and dystroglycan are recruited (Feltri et al., 2002; Berti et al., 2011), and downstream intracellular molecules such as integrin-linked kinase (Ilk; Pereira et al., 2009), focal adhesion kinase (Fak;

The Rockefeller University Press $30.00
J. Exp. Med. 2014 Vol. 211 No. 1 29-43
www.jem.org/cgi/doi/10.1084/jem.20130720

Grove et al., 2007), and the RhoGTPase Rac1 are activated (Benninger et al., 2007; Nodari et al., 2007).

Another pathway originated by neuregulin 1 (Nrg1) type III might be involved in axonal sorting (Raphael et al., 2011). Nrg1 type III is an axonally anchored molecule that interacts with ErbB2/3 receptor on Schwann cells and regulates their proliferation and survival in early development and myelination after birth (Nave and Salzer, 2006; Birchmeier and Nave, 2008). As for Laminin211, Nrg1 signaling may control radial sorting through Schwann cell proliferation and cytoskeletal remodeling (Benninger et al., 2007; Raphael et al., 2011). The molecular basis of laminin- and Nrg1-derived signals and whether they constitute distinct pathways or interact to regulate axon sorting are unclear.

Studies in cancer cells showed that laminin and ErbB2 control the expression and function of Jun activation domain–binding protein 1 (Jab1; Hsu et al., 2007; Wang et al., 2011), a multifunctional protein member of the COP9 signalosome complex. Jab1, shuttling between nucleus and cytoplasm, controls many cell functions such as proliferation, gene transcription, and protein degradation, thus carefully regulating cell number, differentiation, and motility (Chamovitz and Segal, 2001; Shackleford and Claret, 2010). Recently, changes in Jab1 expression have been described in injured peripheral nerves and inversely correlated to $p27^{KIP1}$ (p27), a potent cell cycle inhibitor (Cheng et al., 2013). Thus, Jab1 constitutes a good candidate to integrate laminin211- and Nrg1-derived signals in Schwann cells to regulate axonal sorting.

To investigate Jab1 function in nerve development, we generated and characterized a mouse in which Jab1 was ablated in Schwann cells. Here we report that, consistent with our hypothesis, loss of Jab1 in Schwann cells causes axonal sorting defects leading to a dysmyelinating neuropathy. Our data suggest that Jab1 integrates laminin211- but not Nrg1-derived signals to control p27 levels and to regulate Schwann cell differentiation and cell number. Indeed, p27 levels are increased in Jab1 mutant nerves, and down-regulation of p27 in jab1-null mice restores Schwann cell number and axonal sorting and rescues the peripheral neuropathy.

RESULTS

Jab1 is expressed in the peripheral nerve and timely regulated

To determine whether Jab1 regulates Schwann cell number and axonal sorting, we first investigated Jab1 expression in the peripheral nerve. mRNA and protein were extracted from purified rat Schwann cells, dorsal root ganglia (DRG) sensory neurons, or myelinating Schwann cell/DRG neuron co-cultures and rat sciatic nerves. Jab1 expression was detected in all samples (Fig. 1 A and not depicted), demonstrating that Jab1 is expressed in both Schwann cells and neurons. Jab1 expression is also modulated during nerve development. Jab1 mRNA expression was evaluated at postnatal day (P) 1, P3, P7, P15, and P50 in WT mice. Jab1 mRNA expression showed higher levels of expression in the first postnatal week, as Schwann cells exit from the cell cycle and sort axons, whereas it was down-regulated in adult mice (Fig. 1 B).

Jab1-null mice manifest motor dysfunction

To evaluate Jab1 function in Schwann cells, we generated mice with conditional inactivation of *Jab1* in Schwann cells using the *P0-Cre* transgene. The *P0-Cre* transgene is active from embryonic day (E) 14 in the Schwann cell lineage (Feltri et al., 1999). Genomic PCR analysis showed efficient Cre-mediated recombination (Fig. 1 C), as reported previously (Feltri et al., 2002). Ablation of *Jab1* in Schwann cells was confirmed by immunohistochemistry; Jab1 was no longer detected in nuclei or the cytoplasm of mutant Schwann cells (Fig. 1 D). Western blot of $Jab1^{fl/fl}$ P0-cre (hereafter $Jab1^{-/-}$) sciatic nerve homogenate confirmed a consistent reduction of Jab1 (Fig. 1 E); low residual level of Jab1 likely originated from axons and fibroblasts.

$Jab1^{-/-}$ mice were born in the expected Mendelian ratio and did not show any clinical phenotype at birth. However, 4-wk-old $Jab1^{-/-}$ mice showed clenching of toes when suspended by the tail, suggesting a nerve dysfunction (Fig. 1 F). The sciatic nerve of adult mice also looked thinner and translucent as compared with controls, indicating reduced myelination (Fig. 1 F). By 3–4 mo of life, $Jab1^{-/-}$ mice showed tremor and wide based gait, which worsened with age (Video 1). At 4 mo old, all of the mice showed a complete penetrance of the phenotype. Rotarod analyses of P60 $Jab1^{-/-}$ mice showed significant impairment of motor performance (Fig. 1 G). Neurophysiology clearly showed signs of dysmyelination, as we observed a significant reduction of nerve conduction velocity (NCV; WT 39.5 ± 1.1 vs. $Jab1^{-/-}$ 14.6 ± 1.5 m/s; $n = 10$; $P < 0.0001$) and temporal dispersion of waveforms (Fig. 1 H).

Ablation of Jab1 in Schwann cells impairs axonal sorting

We next examined nerve morphology. Sciatic nerves of P60 WT mice showed that all large axons >1 µm in diameter were sorted into a 1:1 relationship with Schwann cells and were myelinated (Fig. 2 A). Conversely, nerves of $Jab1^{-/-}$ mice showed many unsorted axons, tightly packed in large bundles of mixed caliber axons, some >1 µm, and were entirely surrounded by Schwann cell processes (Fig. 2, B and C, arrows and arrowheads). Some Schwann cells were able to insert processes into axon bundles but were arrested in sorting (Fig. 2 C, bottom). Moreover, Schwann cell basal lamina was sometimes discontinuous (Fig. 2 D, arrows). Other axons achieved appropriate 1:1 relationships with Schwann cells but remained not myelinated (Fig. 2 D) or hypomyelinated. Accordingly, the g ratio was significantly increased in $Jab1^{-/-}$ mice (0.70 ± 0.01; $n = 5$) as compared with controls (0.66 ± 0.01; $n = 5$; $P < 0.0001$; see Fig. 8 C). Sciatic nerves of P90 $Jab1^{-/-}$ mice also showed polyaxonal myelination, and bundles of unsorted axons were entirely myelinated by a single Schwann cell (Fig. 2 E). In 6-mo-old mice, we also observed significant fiber loss (WT 2,407 ± 70 vs. $Jab1^{-/-}$ 617 ± 53 myelinated fibers per mm^2; $n = 4$; $P < 0.05$), with evident signs of axonal and Schwann cell degeneration (Fig. 2 F).

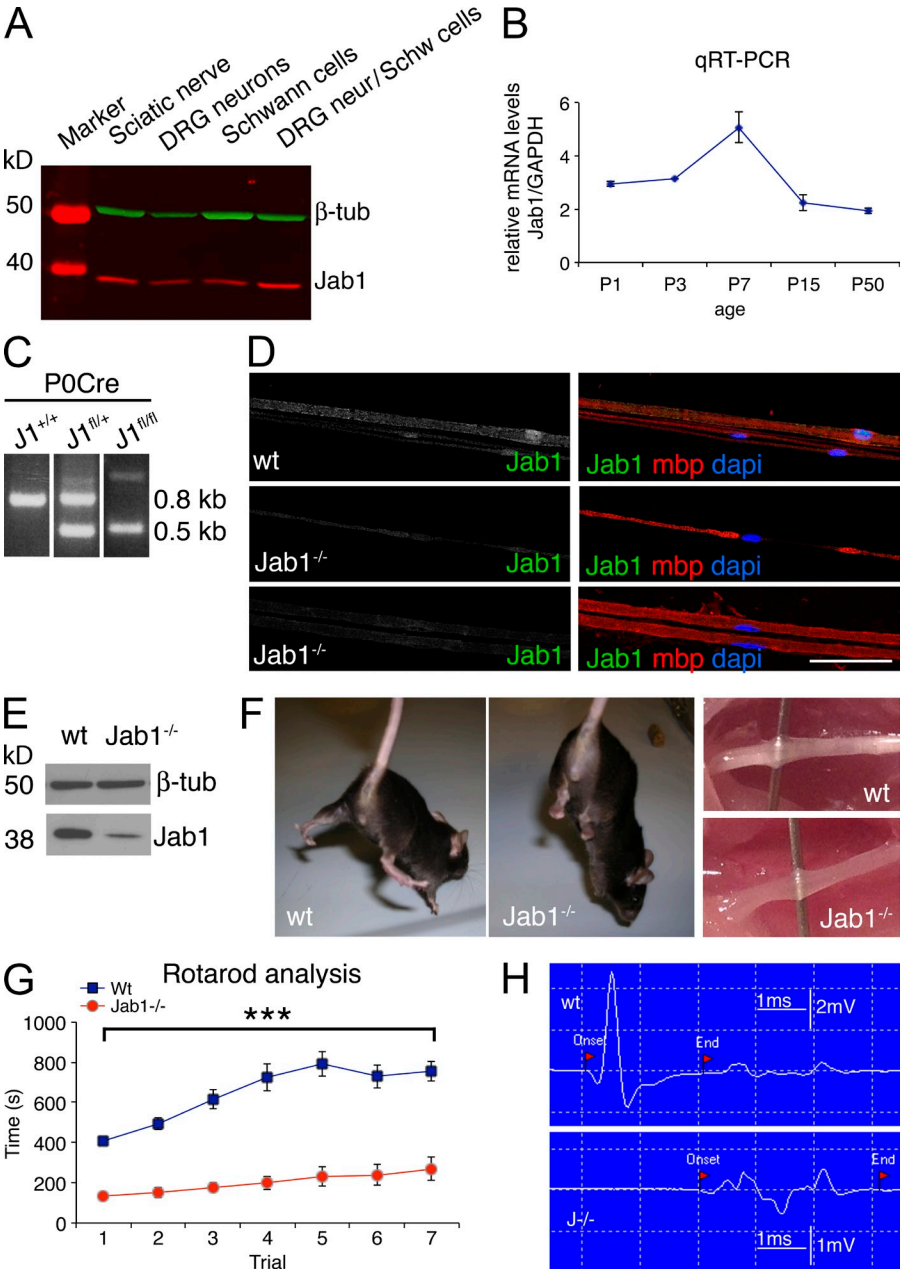

Figure 1. Jab1 expression in peripheral nerves and cre-mediated deletion of Jab1 in Schwann cells. (A) Western blot for Jab1 expression in the homogenate of isolated rat Schwann cells, DRG sensory neurons, co-culture of Schwann cells and DRG neurons, and sciatic nerve. Schwann cell and neuron lysates were obtained after 7 d in culture in defined media, whereas co-cultures were harvested 7 d after supplementation with ascorbic acid to induce myelination. β-Tubulin was used as loading control. (B) Quantitative RT-PCR for the expression of *Jab1* in sciatic nerve during postnatal development. Each time point is the mean of five experiments (each experiment was performed with a pool of five to seven nerves). (C) Genotyping of sciatic nerve genomic DNA isolated from *Jab1*$^{+/+}$ *P0-cre* (WT), *Jab1*$^{fl/+}$ *P0-cre* (*Jab*$^{+/-}$), and *Jab1*$^{fl/fl}$ *P0-cre* (*Jab1*$^{-/-}$) mice. (D) Teased sciatic nerve fibers from P60 WT and *Jab1*$^{-/-}$ mice stained for Jab1 and Mbp. DAPI identifies the nucleus. Bar, 100 µm. (E) Western blot for Jab1 expression in the sciatic nerve homogenate of P5 WT and *Jab1*$^{-/-}$ mice. Representative figure of three independent experiments is shown. (F) Normal hindlimb postural reflex in a P60 WT mouse; abnormal reflex characterized by crossing of the limbs in *Jab1*$^{-/-}$ mouse. Images on the right show the appearance of sciatic nerve at gross examination before dissection in WT and *Jab1*$^{-/-}$ mice. (G) Rotarod analysis of motor function (seven repeated motor trials) in WT and *Jab1*$^{-/-}$ mice; paired Student's *t* test analysis: ***, $P \leq 0.001$; $n = 13$ mice per genotype. (H) Representative traces of sciatic nerve cMAP recorded from foot muscle after distal stimulation. Error bars indicate SEM.

Heterozygous *Jab1*$^{flox/+}$ *P0-cre* mice did not show any morphological or functional alteration (not depicted). In conclusion, the absence of Jab1 in Schwann cells causes a peripheral neuropathy characterized by axonal sorting defects, hypomyelination, and subsequent axonal loss.

To confirm that bundles of unsorted axons are a consequence of altered development, we evaluated sciatic nerves at P1. WT mice, as expected, showed bundles of unsorted axons, although all of them were ensheathed and separated by Schwann cell processes (Fig. 3 A). Conversely, in *Jab1*$^{-/-}$ nerves, bundles already contained tightly associated axons that lacked Schwann cell ensheathment (Fig. 3 A). Of note, sorted and myelinated axons were present similarly in WT and *Jab1*$^{-/-}$ mice (Fig. 3 A), suggesting that loss of Jab1 does not delay myelination. At P5, no more bundles of unsorted axons were observed in WT mice, whereas in *Jab1*$^{-/-}$ nerves the sorting defect was still present, similar to that seen at P1 and in adult nerves (Fig. 3 B). These data confirm that sorting defects of *Jab1*$^{-/-}$ nerves are present from early development.

Jab1-null nerves resemble Lama2 nerves

Radial sorting defects and dysmyelination observed in *Jab1*$^{-/-}$ nerves were similar to those described in mouse mutants for laminins, laminin receptors, and associated molecules (Bradley and Jenkison, 1973; Feltri et al., 2002; Benninger et al., 2007; Grove et al., 2007; Nodari et al., 2007; Pereira et al., 2009). Together with the fact that Jab1 can be modulated by laminins in other cell types (Wang et al., 2011), all

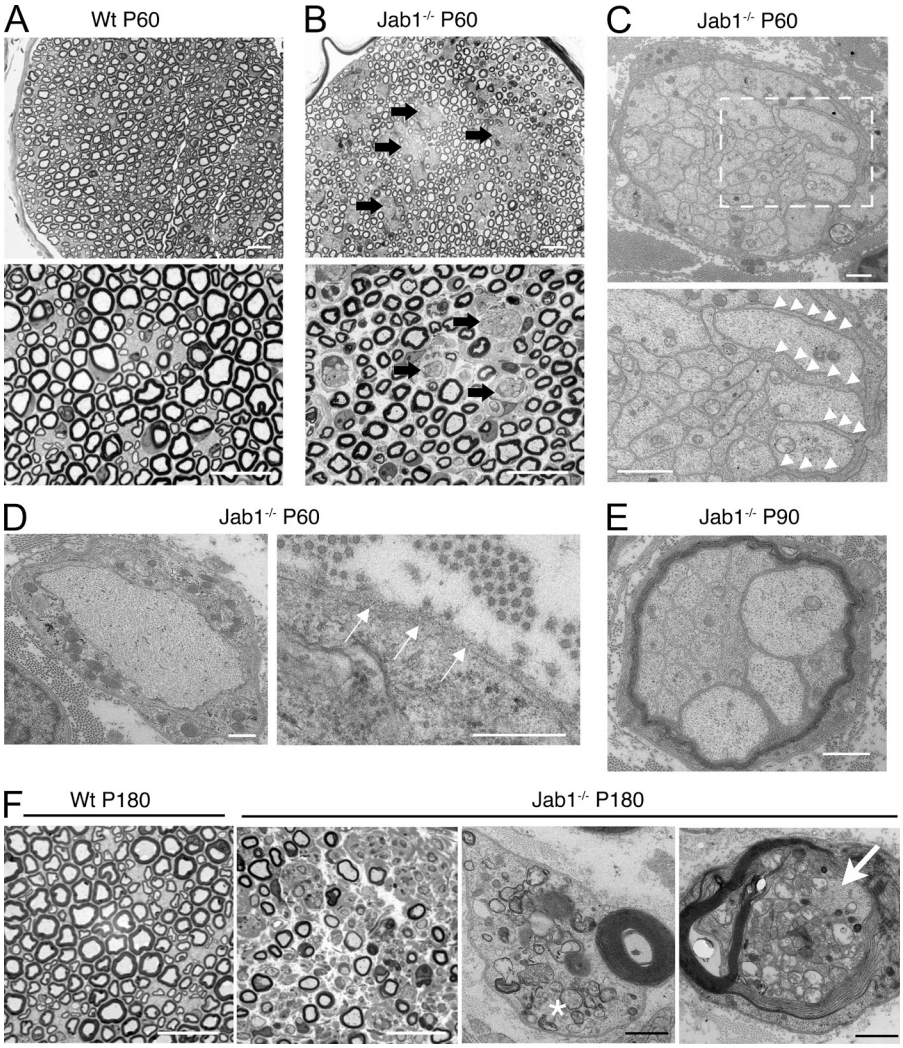

Figure 2. Ablation of Jab1 results in defective axon sorting and myelination. (A and B) Semithin sections of P60 sciatic nerves from WT (A) and *Jab1*$^{-/-}$ (B) mice. Arrows identify bundles of unsorted axons in mutant nerves. (C) Electron micrographs of P60 sciatic nerves from *Jab1*$^{-/-}$ mice. Bundles of unsorted axons contain axons of different caliber, including those with diameter >1 µm. Bundles are entirely surrounded by Schwann cells that protrude processes within the axons; the boxed area is magnified below, and arrowheads identify Schwann cell protrusions within unsorted axons. (D) Electron micrographs of P60 sciatic nerves from *Jab1*$^{-/-}$ mice showing sorted but not myelinated axons and discontinuous basal lamina (arrows). (E) Electron micrographs of P90 sciatic nerves from *Jab1*$^{-/-}$ mice showing bundles of unsorted axons entirely myelinated (polyaxonal myelination). (F) Semithin and ultrathin sections of 6-mo-old sciatic nerve from WT and *Jab1*$^{-/-}$ mice. The asterisk identifies Schwann cell degeneration, and the arrow shows axonal degeneration. Bars: (A, B, and F [left]) 20 µm; (C [top], E, and F [right]) 1 µm; (C, bottom) 1.7 µm; (D) 0.5 µm.

these findings suggest that Jab1 may regulate axonal sorting downstream of laminin211.

To further support this hypothesis, we evaluated whether Jab1 expression was changed in mouse mutants for laminin211 and laminin211 receptors. We performed Western blot analysis for Jab1 in sciatic nerve homogenates of *dy2J* (laminin211 mutant caused by splice mutation of the *lama2* gene that generates a truncated protein; Guo et al., 2003) and *dy3K* (complete null for laminin211; Miyagoe et al., 1997) or mice with conditional inactivation of β1 integrin in Schwann cells (Feltri et al., 2002). We observed significant reduction of Jab1 levels in all mutants when compared with controls (Fig. 4 A). To exclude the possibility that Jab1 down-regulation was simply caused by unspecific dysmyelination and axon degeneration, we evaluated Jab1 expression in two additional mouse models of peripheral neuropathy not related to the laminin 211 pathway: (1) the Fig4$^{-/-}$ (plt/plt) mouse, which is a model of human CMT4J and is characterized by dysmyelination and axonal degeneration (Chow et al., 2007), and (2) the myelin protein zero (Mpz) Ser63del mouse, which is a model of CMT1B and is characterized by dysmyelination and subsequent demyelination (Wrabetz et al., 2006). In both cases, Jab1 expression was not altered (Fig. 4 D and not depicted), further supporting the idea that Jab1 expression is influenced by laminin211.

To further evaluate the relationship between Jab1 and laminin211, we investigated whether laminin211 expression was affected in *Jab1*$^{-/-}$ nerves. Western blot and immunohistochemistry showed significant reduction of laminin211 levels in *Jab1*$^{-/-}$ sciatic nerves (Fig. 4, B and C). Overall, morphological and expression data support the idea that Jab1 functions in the laminin211 pathway.

Jab1 expression is not influenced by Nrg1–ErbB2 signals

Because ErbB signaling plays a role in axonal sorting and myelination (Nave and Salzer, 2006; Raphael et al., 2011), and in cancer cells may control Jab1 expression (Hsu et al., 2007), we investigated whether Nrg1-ErbB2 regulates Jab1 expression also in the peripheral nerve. As *Nrg1 type III*$^{-/-}$ mice are not viable, we investigated Jab1 expression in *Nrg1 type III*$^{+/-}$ mice. Western blot of sciatic nerve homogenates showed similar amounts of Jab1 protein in heterozygous mutants and controls (Fig. 4 E). In addition, Western blot for Jab1 expression in

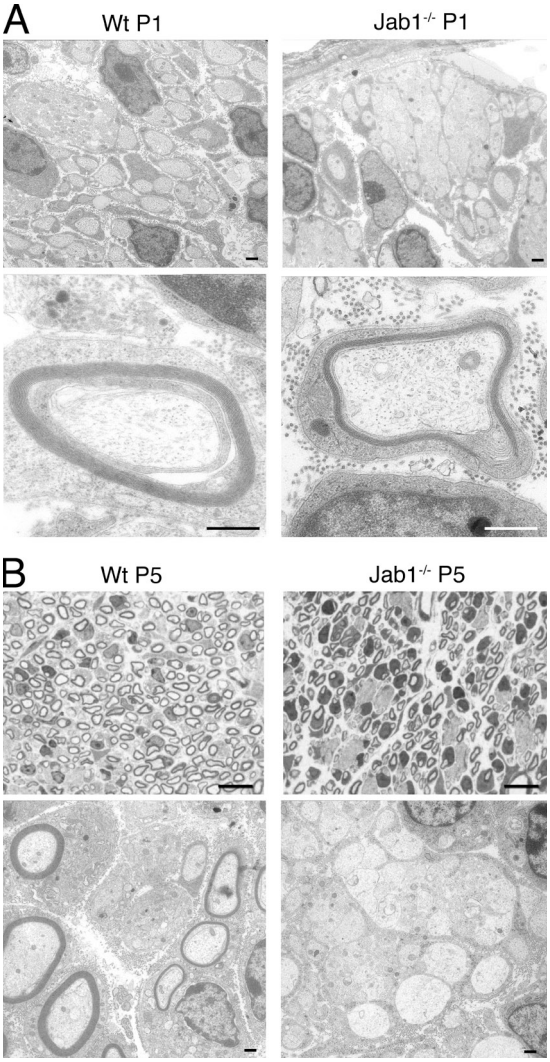

Figure 3. Axonal sorting defect is present since early development. (A) Electron micrographs of sciatic nerve from P1 WT and *Jab1*$^{-/-}$ mice showing bundles of unsorted axons and myelinated fibers. (B) Semithin and ultrathin sections of sciatic nerve from P5 WT and *Jab1*$^{-/-}$ mice showing bundles of unsorted axons only in Jab1$^{-/-}$ nerves. Bars: (A and B [bottom]) 0.5 µm; (B, top) 10 µm.

DRG explants from *Nrg1 type III*$^{-/-}$ or WT mice after 3 and 15 d in culture (supplemented with ascorbic acid) revealed no significant differences (not depicted). Finally, we investigated the activation of the ErbB2 receptor in *Jab1*$^{-/-}$ nerves. If ErbB receptor and Jab1 belong to the same pathway, one might expect abnormal activation of the ErbB2 receptor in *Jab1*$^{-/-}$ mice. Western blot analysis of sciatic nerves of WT and *Jab1*$^{-/-}$ mice showed that ErbB2 expression and phosphorylation were similar (not depicted). Overall, these findings suggest that the Nrg1-ErbB2 signaling pathway does not control Jab1 expression in Schwann cells.

Jab1-null Schwann cells do not differentiate properly

Proper radial sorting is coupled with Schwann cell differentiation (Jessen and Mirsky, 2005). Accordingly, sorting defects have been associated with delayed or arrested Schwann cell differentiation (Chen and Strickland, 2003; Benninger et al., 2007). Thus, we investigated the Schwann cell differentiation markers c-Jun, Oct6, and Krox20 in *Jab1*$^{-/-}$ sciatic nerves. Immunohistochemistry at P5 and P15 showed that Oct6 expression was significantly increased, whereas Krox20 expression was significantly decreased as compared with controls (Fig. 5 A). In parallel, total levels of c-Jun and phosphorylated c-Jun were significantly increased in *Jab1*$^{-/-}$ sciatic nerve homogenate (Fig. 5 B). Overall, these results reveal defective differentiation of *Jab1*$^{-/-}$ Schwann cells.

Loss of Jab1 impairs Schwann cell cycle and survival

Despite radial sorting defects and defective Schwann cell differentiation in *Jab1*$^{-/-}$ nerves, mutant Schwann cells attempted to send processes within axon bundles and associated with sorted axons, similar to *Cdc42* and *Fak* mutants. Insufficient numbers of Schwann cells as a consequence of reduced proliferation or survival was proposed to cause the axonal sorting defect in them (Benninger et al., 2007; Grove et al., 2007). As Jab1 modulates the cell cycle in other cell types (Chamovitz and Segal, 2001), we investigated Schwann cell number, survival, and cell cycle progression in *Jab1*$^{-/-}$ nerves.

Consistent with our hypothesis, the number of Schwann cells in *Jab1*$^{-/-}$ nerves was significantly reduced as compared with WT nerves, from E15.5 to adulthood (Fig. 6 A). TUNEL assay for Schwann cell death showed no differences between *Jab1*$^{-/-}$ and WT mice until P1. At P5, however, we observed a significant increase in the percentage of TUNEL-positive cells in mutant nerves as compared with controls (Fig. 6 B).

However, apoptosis in *Jab1*$^{-/-}$ nerves at P5 would not explain the reduced Schwann cell number observed in prenatal development. Thus, we investigated Schwann cell proliferation and cell cycle progression by double labeling with BrdU and Ki67. Single-pulse BrdU identified Schwann cells in S phase, whereas Ki67 marked Schwann cells in all active phases of cell cycle (G1-S-G2-M phase; scheme in Fig. 6 D), allowing us to estimate whether Schwann cells were actively proliferating or arrested in the cell cycle. Single staining for Ki67 did not show differences in Schwann cell proliferation at any time point between *Jab1*$^{-/-}$ and WT nerves, whereas BrdU incorporation was somewhat higher, although not significant, in mutants (Fig. 6 C). However, when we performed double labeling with Ki67 and BrdU at E17.5 and P5, we observed that only roughly 50% of Schwann cells were double positive in normal nerves, thus being in S–early G2 phase. On the contrary, in *Jab1*$^{-/-}$ nerves the majority of Schwann cells were double positive for Ki67 and BrdU, suggesting that they entered into the cell cycle but then accumulated in S–early G2 phase (Fig. 6 D). At P30, this difference, although still present, was not significant.

To confirm that *Jab1*$^{-/-}$ Schwann cells were defective in S-G2 phase progression, we measured levels of cyclin A, B1, D1, and E by Western blot in P5 sciatic nerves. Cyclin D1 is expected to be high in G1 and G2 phase, cyclin E in G1 and S phase, cyclin A in S and early G2 phase, and cyclin B1 in late

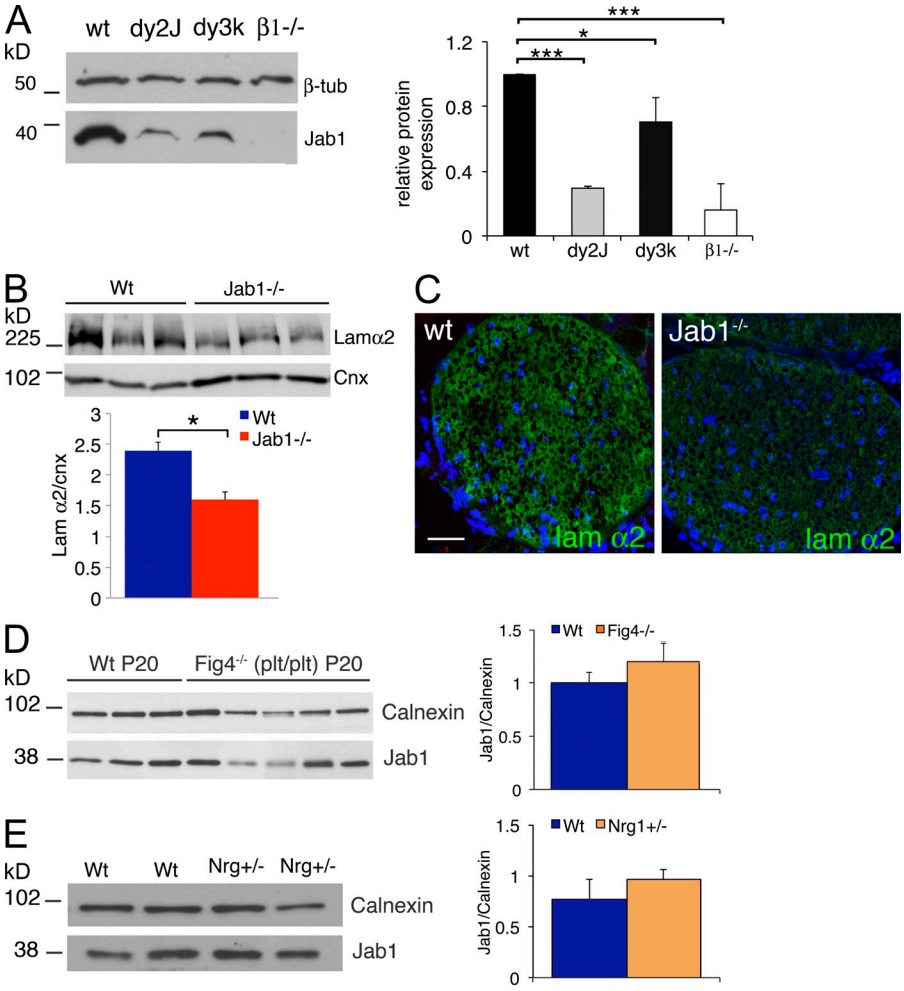

Figure 4. Laminin211 and Jab1 influence each other's expression. (A) Western blot for Jab1 protein in sciatic nerve homogenate of WT (P30), *dy2J* (P30), *dy3K* (P20), and β1 integrin$^{-/-}$ (P30) mice. Quantification is reported as the mean of three different mice per genotype (three independent experiments) and represented as ratio Jab1/β-tubulin, assigning WT as 1. (B) Western blot for laminin chain α2 in sciatic nerve homogenate of WT and *Jab1*$^{-/-}$ mice. Quantification is reported as the mean of three different mice per genotype) and represented as ratio laminin chain α2/calnexin. (C) Immunofluorescence staining for laminin chain α2 in P20 sciatic nerves of WT and *Jab1*$^{-/-}$ mice. Bar, 50 µm. (D) Western blot for Jab1 in sciatic nerve homogenate of P20 WT and Fig4$^{-/-}$ (plt/plt) mice. Quantification is reported as the mean of three different mice for WT and five mice for Fig4$^{-/-}$. (E) Western blot for Jab1 in sciatic nerve homogenate of P30 WT and Nrg1 type III$^{+/-}$ mice. Quantification is reported as the mean of two different mice per genotype. (D and E) Calnexin was used as a loading control. Unpaired Student's *t* test in A and paired Student's *t* test in B, D, and E: *, P ≤ 0.05; ***, P ≤ 0.001. Error bars indicate SEM.

G2–M phase (Bardin and Amon, 2001). In agreement with the BrdU/Ki67 results, we found higher levels of cyclin D1, E, and A in nerve homogenates of *Jab1*$^{-/-}$ mice, whereas levels of cyclin B1 were similar to controls (Fig. 6 E). All these data demonstrate that *Jab1*$^{-/-}$ Schwann cells enter into the cell cycle but then present a defective progression in S-G2 phase. Overall, our results indicate that *Jab1*$^{-/-}$ Schwann cells do not properly differentiate, are defective in cell cycle progression, and eventually undergo apoptosis, resulting in significantly reduced numbers of Schwann cells during nerve development.

Deficient Schwann cell number in Jab1$^{-/-}$ nerves is caused by abnormal p27 levels

Cyclin-dependent kinase inhibitors such as p27, p21, and p16 are major negative regulators of cell cycle progression in glial cells (Stevens and Fields, 2002). Previous studies showed that loss of p21 or p16 in mice does not alter peripheral nerve formation or embryonic and perinatal Schwann cell proliferation (Atanasoski et al., 2006). Although there are no in vivo loss of function studies of p27 in Schwann cells, increased levels of p27 are associated with cell cycle arrest in oligodendrocytes and Schwann cells (Casaccia-Bonnefil et al., 1999; Li et al., 2011). As Jab1 has been shown to control p27 levels in other cell types (Shackleford and Claret, 2010), and its expression inversely correlates with p27 in injured nerve (Cheng et al., 2013), we hypothesized that defective Schwann cell cycle progression in *Jab1*$^{-/-}$ mice was caused by high p27 levels. Accordingly, p27 was increased in P5 and P30 mutant nerve homogenates by Western blot analysis (Fig. 6 F and not depicted). Thus, defective Schwann cell number and cell cycle progression observed in *Jab1*$^{-/-}$ mice correlate with increased p27 levels.

p27-null mice do not show abnormal peripheral nerves

To further confirm that the axonal sorting defect in *Jab1*$^{-/-}$ mice was caused by high p27 levels, we analyzed *Jab1*$^{-/-}$*p27*$^{-/-}$ double mutant mice for a rescue of this defect. As a control, adult (P30) *p27*$^{-/-}$ sciatic nerves did not show abnormalities in axonal sorting, axon number, fiber size distribution, and myelination (g ratio WT 0.678 ± 0.01 vs. mutants 0.673 ± 0.01; $n = 3$; P = not significant; Fig. 7 A). Similarly, neurophysiology did not show differences in compound motor action potential (cMAP; WT 9.7 ± 1.4 vs. mutant 12.2 ± 3.0 mV; $n = 4$; P = not significant) or NCV (WT 37.8 ± 2.0 vs. mutant 37.3 ± 1.8 m/s; $n = 4$; P = not significant).

We then analyzed Schwann cell number, survival, and differentiation in *p27*$^{-/-}$ sciatic nerves during development. At

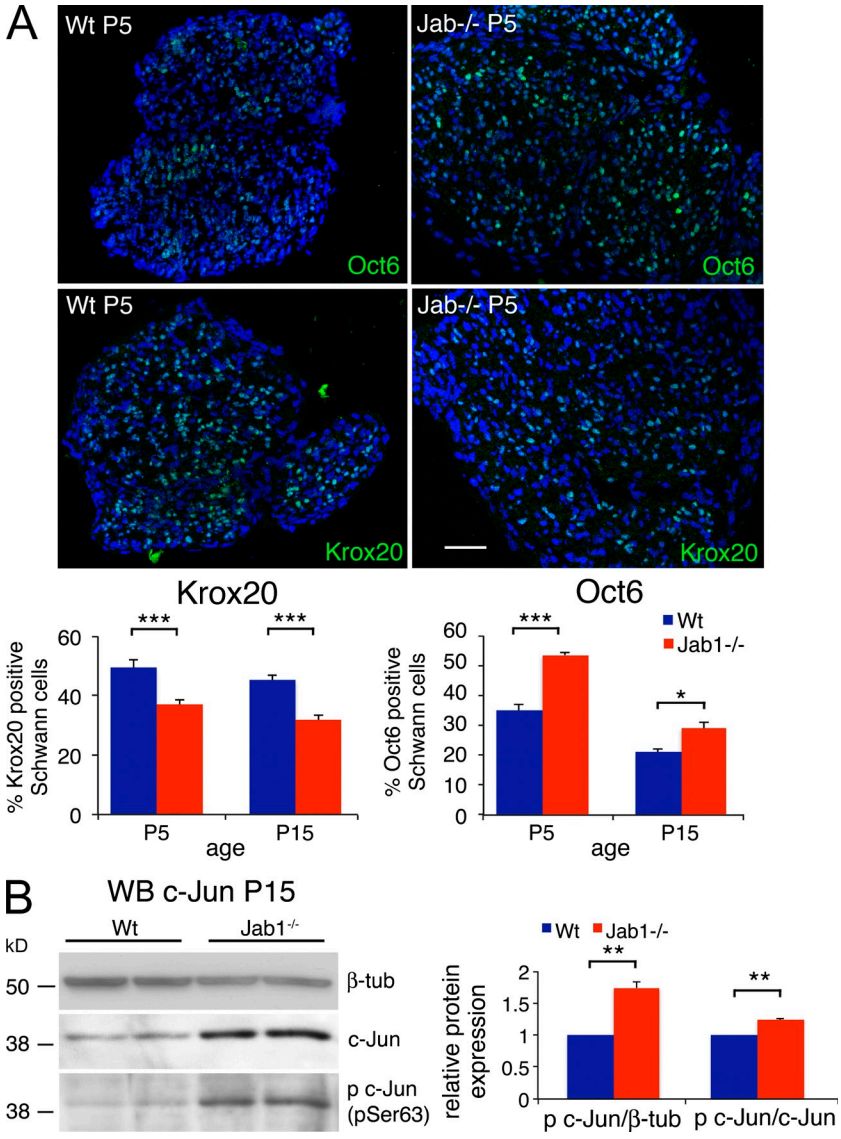

Figure 5. Schwann cells in mutant nerves show abnormal differentiation. (A) Quantification of Oct6- and Krox20-positive nuclei in transverse sciatic nerve sections of P5 and P15 WT and *Jab1*$^{-/-}$ mice (n = 5 per genotype per time point). Immunofluorescence at P5 is shown as a representative image. Bar, 50 µm. (B) Western blot for c-Jun and phosphorylated c-Jun (p c-Jun) in sciatic nerve homogenate of P15 WT and *Jab1*$^{-/-}$ mice. Quantification is reported as the mean of three different mice per genotype and represented as a ratio of phospho c-Jun/β-tubulin and phospho c-Jun/c-Jun, assigning WT as 1. Paired Student's t test: *, P ≤ 0.05; **, P ≤ 0.01; ***, P ≤ 0.001. Error bars indicate SEM.

P5, Schwann cell number was slightly but significantly increased in *p27*$^{-/-}$ nerves (Fig. 7 B). The proliferation rate measured by Ki67 and BrdU analysis was also slightly increased in mutant nerves, although not significantly, and no differences were observed in cell cycle progression (Fig. 7 B). Furthermore, Schwann cell differentiation was not affected by loss of p27, as we did not observe significant differences in the expression of Oct6 and Krox20 between *p27*$^{-/-}$ and WT mice (Fig. 7 C).

As we observed a slight increase of Schwann cell number in *p27*$^{-/-}$ nerves, we evaluated whether the internodal length was shorter, as described in mouse mutants for p21 and p16 (Atanasoski et al., 2006). Although the number of Schwann cells with internodal length between 500 and 600 µm was reduced in *p27*$^{-/-}$ nerves, we did not detect any significant difference between *p27*$^{-/-}$ and WT nerves (Fig. 7 D). Overall, these data support the idea that reduced p27 levels do not interfere with development and function of peripheral nerve.

Schwann cell number and axonal sorting are restored in Jab1$^{-/-}$ nerves by genetic depletion of p27

To test the hypothesis that abnormal radial sorting in *Jab1*$^{-/-}$ nerves is mostly the consequence of increased p27 levels and defects in Schwann cell cycle progression, we ablated p27 from *Jab1*$^{-/-}$ mice. Notably, adult *Jab1*$^{-/-}$*p27*$^{-/-}$ mice showed a significant rescue of the sorting defect and dysmyelination (Fig. 8 A). We observed that the endoneurial area occupied by bundles was significantly reduced in *Jab1*$^{-/-}$*p27*$^{-/-}$, as well as the mean size of bundles and the number of axons per bundle (Fig. 8, A and B). As an increased number of axons are sorted out of bundles, the number of myelinated axons was also significantly increased (Fig. 8 B).

Distribution of axons when plotted against diameter did not show significant differences between groups (Fig. 8 C), but we observed rescue of hypomyelination. The g-ratio value in double mutants was significantly reduced as compared with *Jab1*$^{-/-}$ mice, and it was similar to WT mice (WT 0.656 ± 0.009,

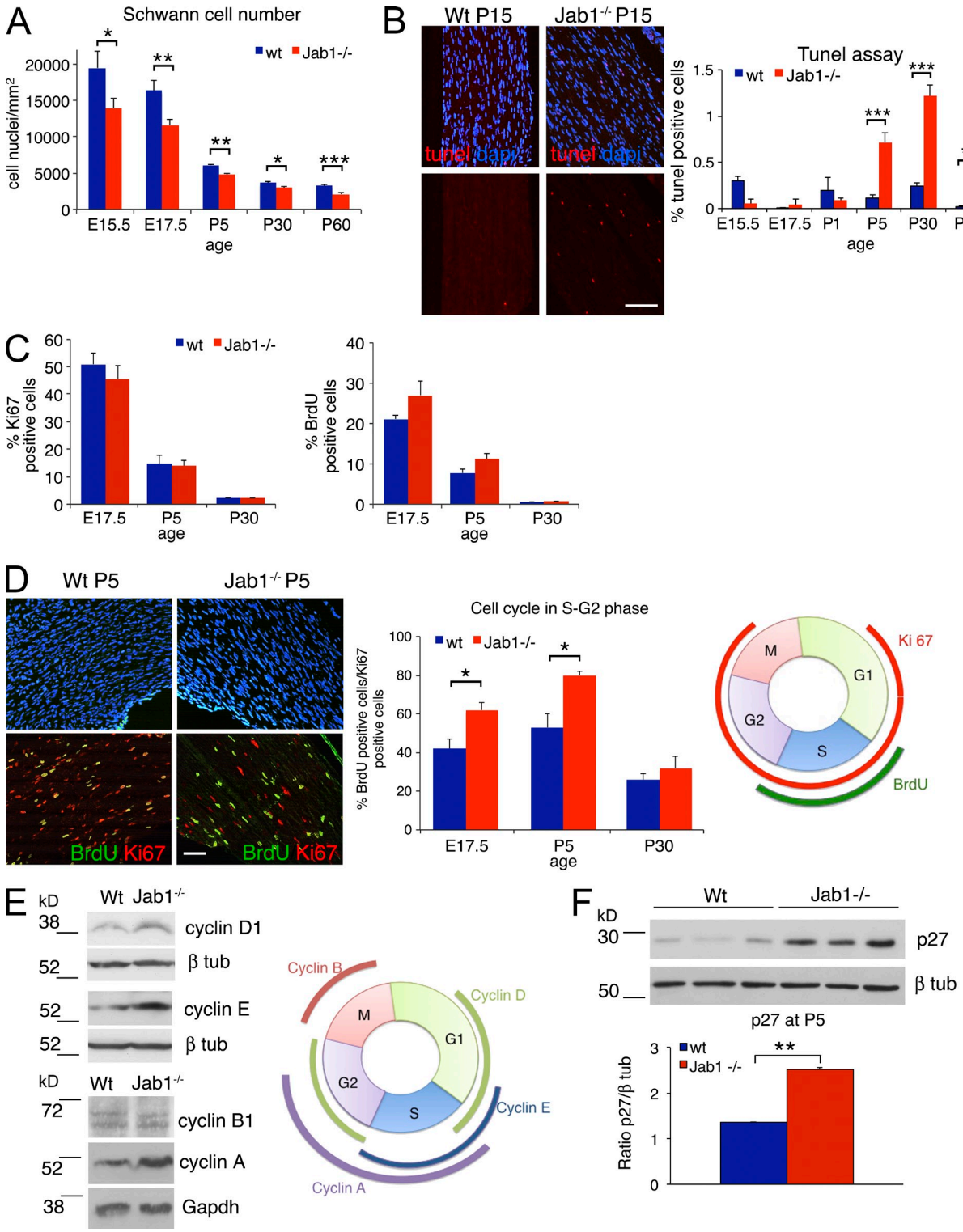

Figure 6. Schwann cells in mutant nerves are reduced in number and defective in cell cycle progression. (A) Quantification of Schwann cell number (S100 positive) in sciatic nerves of WT and *Jab1*$^{-/-}$ mice from E15.5 to P60 (n = 3 mice per genotype per time point). (B) Quantification of TUNEL-positive cells in sciatic nerve sections of WT and *Jab1*$^{-/-}$ mice from E15.5 to P60 (n = 4 mice per genotype per time point); immunofluorescence for TUNEL staining at P15 is shown as a representative image. (C) Quantification of Ki67- or BrdU-positive Schwann cells in sciatic nerves of WT and *Jab1*$^{-/-}$ mice at different time points (n = 3 mice per genotype). (D) Immunofluorescence representative for DAPI, BrdU, and Ki67 staining in sciatic nerves of WT and *Jab1*$^{-/-}$ mice at P5. The percentage of double-positive nuclei (BrdU/Ki67) on the total of Ki67-positive nuclei is quantified at E17.5, P5, and P30 (n = 3 mice per genotype per time point). A schematic representation of the cell cycle and phases marked by Ki67 and BrdU staining are shown on the right.

Jab1$^{-/-}$ 0.705 ± 0.01, *Jab1*$^{-/-}$*p27*$^{-/-}$ 0.665 ± 0.005; P = 0.03 between *Jab1*$^{-/-}$ and *Jab1*$^{-/-}$*p27*$^{-/-}$; $n = 5$; Fig. 8 C). Consistently, we observed functional rescue by neurophysiology, as both NCV and cMAP (significantly reduced in *Jab1*$^{-/-}$ mice) were restored to normal levels in *Jab1*$^{-/-}$*p27*$^{-/-}$ mice (Fig. 8 D).

Finally, we evaluated whether genetically reduced levels of p27 in *Jab1*$^{-/-}$*p27*$^{-/-}$ mice also restored Schwann cell number and cycle progression. At P5, Schwann cell number was significantly rescued toward a normal level (Fig. 8 E), as well as the percentage of Schwann cells double positive for BrdU and Ki67 (Fig. 8 F).

DISCUSSION

Sorting and segregation of axons from bundles is a crucial event during nerve development, as it is necessary for subsequent ensheathment and myelination (Webster et al., 1973; Webster, 1993), whereas if impaired, it results in dysmyelinating neuropathies (Bradley and Jenkison, 1973; Stirling, 1975; Shorer et al., 1995). Here we demonstrate that Jab1 is a key molecule in the regulation of radial sorting of axons. Through the control of p27 levels, Jab1 may transduce laminin211 signals in Schwann cells to regulate withdrawal from the cell cycle, and thus Schwann cell number and differentiation.

Axonal sorting depends on (a) proper Schwann cell differentiation, (b) control of Schwann cell proliferation and survival, as their numbers must exceed a threshold for proper axonal sorting, and (c) cytoskeleton remodeling to extend Schwann cell process, to segregate large caliber axons (Webster et al., 1973; Feltri and Wrabetz, 2005; Jessen and Mirsky, 2005). All of these events are regulated by laminin211, which, together with laminin411, is the key molecule in the control of axonal sorting. Accordingly, spontaneous or knockout mice for laminin211 (and laminin411) present axonal sorting defects (Bradley and Jenkison, 1973; Yang et al., 2005; Yu et al., 2005). During axonal sorting, Laminin211 regulates Schwann cell proliferation, survival, and differentiation likely through the interaction with the laminin receptor β1 integrin and the downstream effector *Fak* (Yang et al., 2005; Yu et al., 2005; Grove et al., 2007; Berti et al., 2011). Moreover, laminin211 is also involved in cytoskeleton remodeling to extend Schwann cell processes, through the interaction with β1 integrin and the downstream effectors Ilk and Rac1 (Benninger et al., 2007; Nodari et al., 2007; Pereira et al., 2009). A few studies suggest that Nrg1 type III might also be involved in axonal sorting. Nrg1 may control Schwann cell proliferation through Cdc42, as conditional inactivation of Cdc42 in Schwann cells impairs axonal sorting (Benninger et al., 2007). Furthermore, by using small molecule inhibitors in zebrafish, it was recently shown that ErbB signals are necessary for Schwann cell process extension during axonal sorting (Raphael et al., 2011). Overall, these findings suggest that both laminins and Nrg1-derived signals may influence Schwann cell behavior during axonal sorting. However, which other downstream molecules are involved and how these extracellular signals are transduced in the Schwann cell to coordinate Schwann cell proliferation, differentiation, and cytoskeleton remodeling remain mostly unknown.

Evidence from other cell types shows that Jab1, shuttling between the nucleus and cytoplasm, regulates cell proliferation and differentiation (Shackleford and Claret, 2010). As laminins and ErbB2-derived signals can control Jab1 function (Hsu et al., 2007; Wang et al., 2011), we hypothesized that Jab1 might have a role in axonal sorting. Our results clearly show that Jab1 plays a key role in axonal sorting by acting downstream of laminin211. In fact, (a) loss of Jab1 causes axonal sorting defects that phenocopy those of laminin211 mutants (Xu et al., 1994; Miyagoe et al., 1997; Nakagawa et al., 2001; Guo et al., 2003), and (b) Jab1 expression is significantly altered in mice lacking laminin211 or its receptor (β1 integrin). Jab1 reduction in mutants for laminin211 is not simply caused by dysmyelination (which is the main feature of young *dy2J* and *dy3K* mice) or axonal loss (present in conditional *β1*$^{-/-}$ mice), as Jab1 expression is not altered in other mouse models for peripheral neuropathy not related to laminin211. In fact, normal Jab1 expression was observed in *Fig4*$^{-/-}$ mice, characterized by dysmyelination and axonal loss (Chow et al., 2007), or in Mpz *Ser63del* mice, characterized by dysmyelination and demyelination (Wrabetz et al., 2006). Moreover, even loss of *Nrg1* does not alter Jab1 expression. Interestingly, laminin211 is significantly reduced in *Jab1*$^{-/-}$ nerves, which also show basal lamina abnormalities similar to laminin211 mutants (Bray et al., 1983), suggesting a bidirectional relationship between Jab1 and laminin211. Reduced levels of laminin211 in *Jab1*$^{-/-}$ nerves may be the consequence of diverse mechanisms. Jab1 may directly control extracellular matrix composition and remodeling, as already reported for collagenase synthesis in fibroblasts (Levinson et al., 2004). Moreover, as molecules that belong to the adhesion pathway, Jab1 may affect inside-out signaling by regulating surface receptors. Indeed, we observed abnormal expression of laminin211 receptors (β-dystroglycan and β1 integrin) in *Jab1*$^{-/-}$ nerves (unpublished data), which may affect extracellular matrix composition and laminin211 organization, as described elsewhere (Henry et al., 2001).

How does Jab1 control axonal sorting downstream of laminin211? Our results indicate that Jab1 controls axon sorting by regulating Schwann cell number (and differentiation) through p27 levels. In fact, *Jab1*$^{-/-}$ nerves show reduced Schwann cell number and increased p27 levels, whereas genetic reduction

(E) Western blot for cyclin levels in sciatic nerve homogenate of P5 WT and *Jab1*$^{-/-}$ mice. Each lane is a pool of 5 sciatic nerves for cyclin D1 and E or 10 sciatic nerves for cyclin B1 and A. The image is representative of two independent experiments. A schematic representation of cyclin expression in the different phases of cell cycle. (F) Western blot for p27 in sciatic nerve homogenate of P5 WT and *Jab1*$^{-/-}$ mice. Quantification is reported as the mean of three different mice per genotype and represented as ratio p27/β-tubulin. Paired Student's *t* test: *, P ≤ 0.05; **, P ≤ 0.01; ***, P ≤ 0.001. Error bars indicate SEM. Bars: (B) 50 µm; (D) 30 µm.

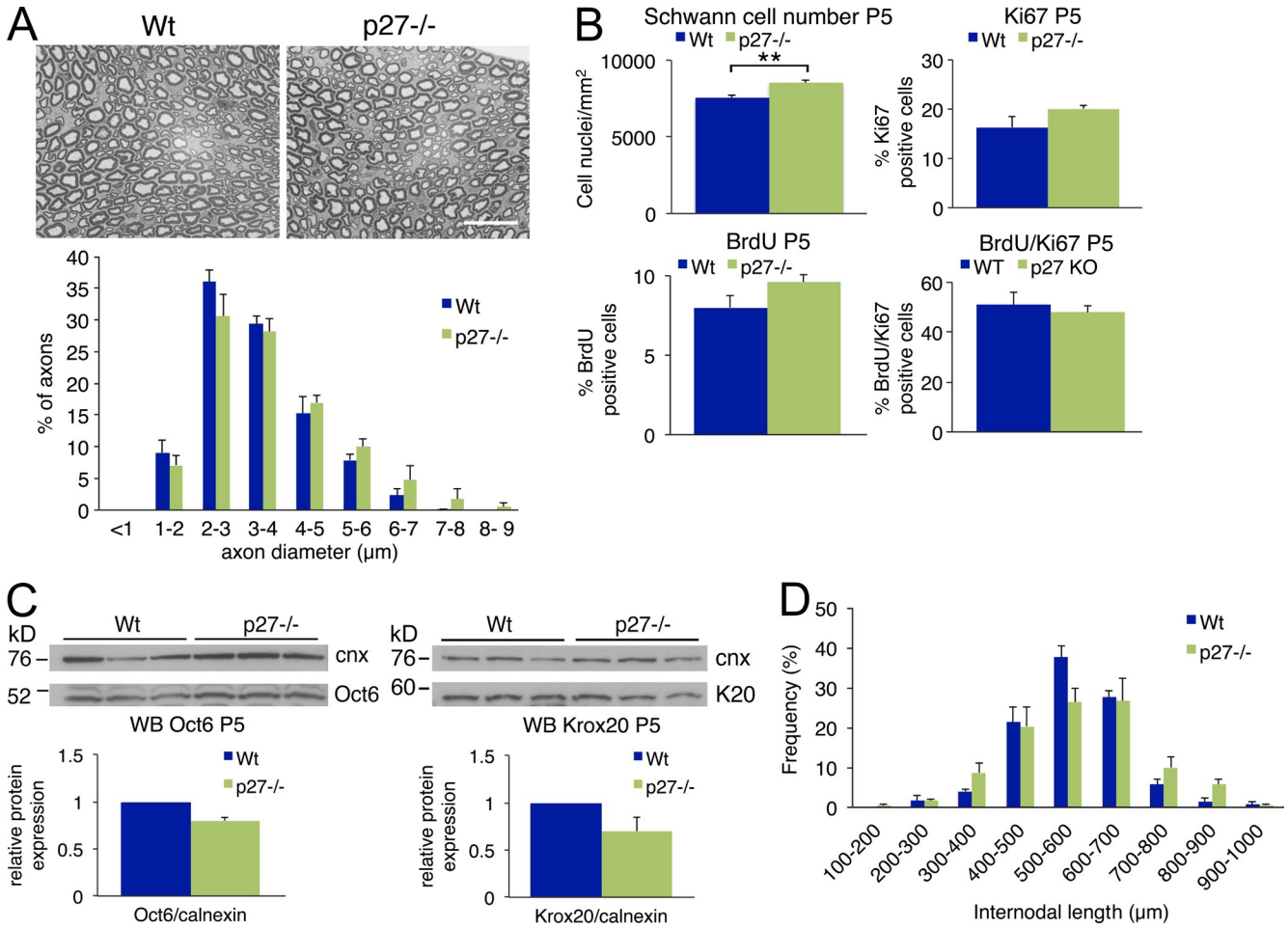

Figure 7. Loss of p27 does not alter nerve development. (A) Semithin sections of sciatic nerve from P60 WT and *p27*$^{-/-}$ mice and fiber type distribution per axon diameter. Bar, 20 µm. (B) Quantification of Schwann cell number and percentage of BrdU-, Ki67-, and double BrdU/Ki67-positive staining in nerves of P5 WT and *p27*$^{-/-}$ mice (n = 3 mice per genotype per experiment). (C) Western blots for Oct6 and Krox20 in sciatic nerve homogenate of P5 WT and *p27*$^{-/-}$ mice. Calnexin was used as a loading control. Quantification is reported as the mean of three independent mice per genotype and represented as ratio Oct6 or Krox20/calnexin, assigning WT as 1. (D) Internodal length of P30 WT and *p27*$^{-/-}$ sciatic nerve (n = 100 fibers per mouse, three mice per genotype). Paired Student's t test: **, P ≤ 0.01. Error bars indicate SEM.

of p27 in *Jab1*$^{-/-}$ mice almost rescues Schwann cell number, differentiation, and the axonal sorting defect. Consistent with our hypothesis, we observed a significant reduction in Schwann cell number from early nerve development (E15.5) in *Jab1*$^{-/-}$ mice. We then expected to observe a reduced rate of proliferation, as Schwann cell survival was altered only postnatally in mutant mice. Surprisingly, both Ki67 staining and BrdU incorporation were not significantly different. However, when we analyzed the number of Schwann cells double positive for Ki67 and BrdU on the total number of cycling Schwann cells (Ki67 positive), we clearly observed that most of *Jab1*$^{-/-}$ cycling Schwann cells were also BrdU positive. This indicates that *Jab1*$^{-/-}$ Schwann cells incorporate BrdU but then present defective progression in S phase (or early G2 phase, as we collected nerves 1 h after BrdU injection). In fact, mutant Schwann cells behave differently than WT Schwann cells, which incorporate BrdU and then progress in the cell cycle, as we found WT Schwann cells equally distributed in all of the cycle phases (G1, S, M, and G2). The increased levels of cyclin proteins specific of S-G2 phase revealed in *Jab1*$^{-/-}$ nerves confirmed this result. Thus, our findings sustain Jab1 as the nuclear target of laminin211 signals that, regulating p27 levels, controls Schwann cells cycle progression and number. Accordingly, Jab1 regulates p27 levels in other cell types (Tomoda et al., 2002), and it can physically interact with p27 in Schwann cells (Cheng et al., 2013). Interestingly, abnormal p27 levels affect nerve development only when p27 is elevated in Schwann cells. Indeed, low p27 levels do not alter Schwann cell and nerve development, as previously reported for equivalent molecules such as p21 and p16 (Atanasoski et al., 2006).

Schwann cell proliferation and differentiation are closely linked. In fact, regulated Schwann cell exit from the cell cycle is a prerequisite for Schwann cell differentiation during nerve development and regeneration (Stevens and Fields, 2002) and is modulated by p27 levels (Li et al., 2011). Our results suggest that high p27 levels in *Jab1*$^{-/-}$ mice may withdraw immature

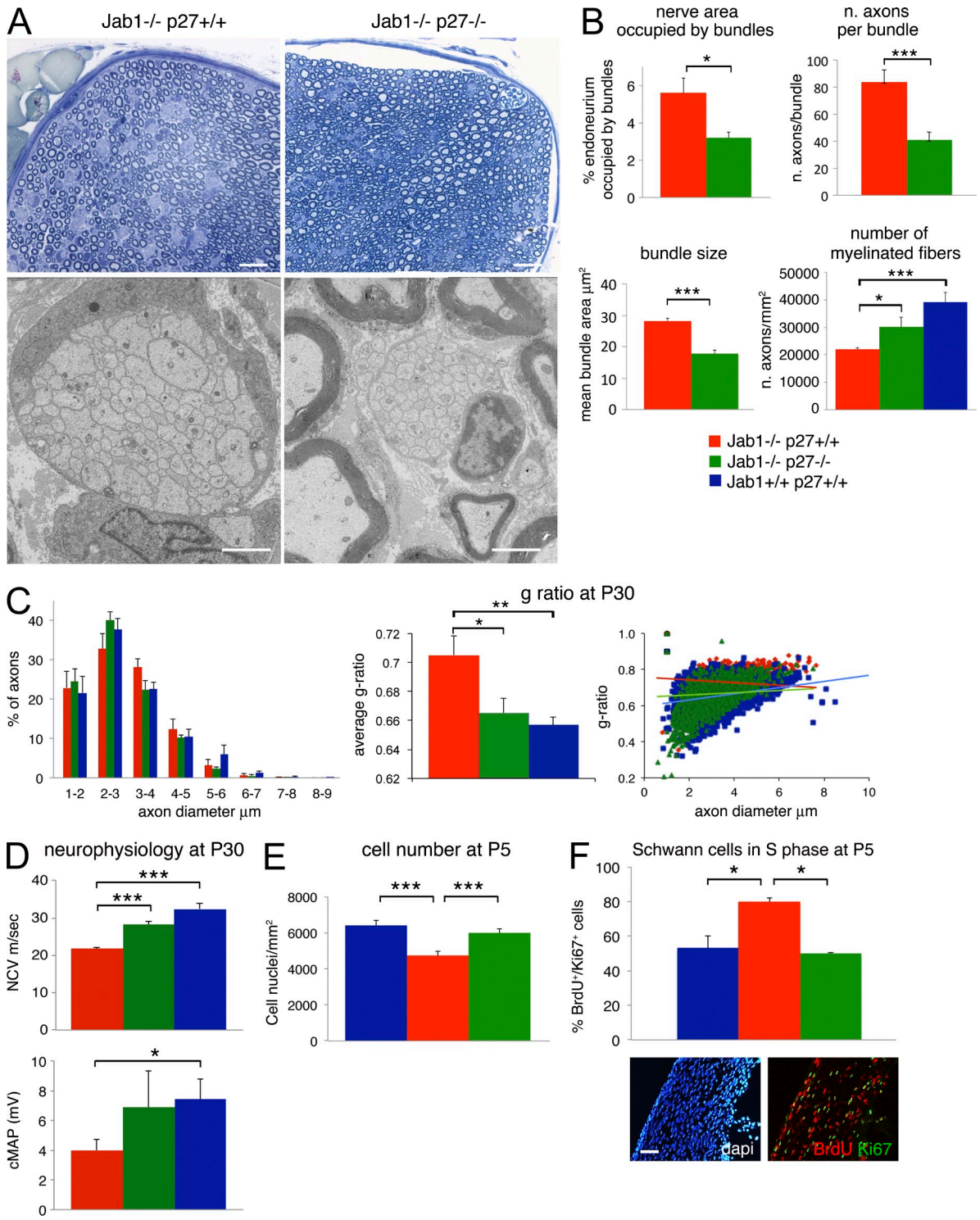

Figure 8. Reduced levels of p27 rescue the peripheral nerve phenotype in Jab1-null mice. (A) Semithin and ultrathin sections of sciatic nerve from P30 *Jab1*$^{-/-}$ and double *Jab1*$^{-/-}$*p27*$^{-/-}$ mice. (B) Morphometric analysis of the endoneurial area occupied by bundles of unsorted axons, number of axons per each bundle, mean bundle size, and number of sorted myelinated axons in *Jab1*$^{-/-}$ and double *Jab1*$^{-/-}$*p27*$^{-/-}$ mice (n = 3 mice per genotype). (C) Analysis of fiber type distribution per axon diameter, mean g ratio, and g ratio per axon diameter in WT (n = 3 mice per genotype) and *Jab1*$^{-/-}$ and double *Jab1*$^{-/-}$*p27*$^{-/-}$ mice (n = 5 mice per genotype). (D) Neurophysiology showing NCV and cMAP in P30 WT, *Jab1*$^{-/-}$, and double *Jab1*$^{-/-}$*p27*$^{-/-}$ mice (n = 3 mice per genotype). (E) Quantification of Schwann cell number in P5 sciatic nerves of WT, *Jab1*$^{-/-}$, and *Jab1*$^{-/-}$*p27*$^{-/-}$ mice (n = 3 mice per genotype). (F) Percentage quantification of nuclei double positive for BrdU and Ki67 staining on the total number of Ki67-positive nuclei in sciatic nerve sections of P5 WT, *Jab1*$^{-/-}$, and *Jab1*$^{-/-}$*p27*$^{-/-}$ mice (n = 3 mice per genotype). A representative immunofluorescence image of *Jab1*$^{-/-}$*p27*$^{-/-}$ mice is shown. Bars: (A, top) 20 µm; (A, bottom) 2 µm; (F) 30 µm. Paired Student's t test: *, P ≤ 0.05; **, P ≤ 0.01; ***, P ≤ 0.001. Error bars indicate SEM.

Schwann cells from the cell cycle. These Schwann cells first arrested in the differentiation program and then, upon different environmental cues, may undergo aberrant differentiation and/or apoptosis. In fact, we clearly observed delayed differentiation in *Jab1*$^{-/-}$ nerves (increased Oct6 and c-Jun and reduced Krox20 positivity), as well as increased apoptosis in postnatal nerve development. However, we also observed polyaxonal myelination, which represents Schwann cells that prematurely myelinate bundles of unsorted axons, suggesting premature differentiation. Thus, proper control of Jab1 and p27 levels regulates not only Schwann cell cycle but also differentiation. Accordingly, high p27 levels are induced in differentiating Schwann cells by axonal signals, whereas inhibition of p27 abolishes the expression of promyelinating markers in Schwann cells (Li et al., 2011). Similarly, increased p27 levels enhance Mbp promoter activity in oligodendrocytes, to leave the cell cycle and begin differentiation (Wei et al., 2003). Interestingly, polyaxonal myelination has also been described in mice deficient of laminin211 and 411 (Yang et al., 2005), further strengthening the relationship between laminins and Jab1.

We cannot completely exclude the possibility that Jab1 also plays a role in cytoskeleton remodeling during axonal sorting. However, *Jab1*$^{-/-}$ Schwann cells can form and extend processes within bundles and myelinate axons when sorted (included unsorted bundles). As loss of Jab1 alters p27 levels, and p27 may interfere with RhoGTPase (Larrea et al., 2009), the possible role of Jab1 in cytoskeleton rearrangement and Schwann cell protrusions will be the subject of future work.

In conclusion, Jab1 may constitute the regulatory molecule that, through the control of p27 levels, governs Schwann cell number and differentiation and integrates into the nucleus the modulatory signals originated by laminin211. Mutations of the human gene *LAMA2*, encoding for the α2 subunit of laminin211, are responsible for MDC1A-associated neuropathies (Shorer et al., 1995; Mercuri et al., 1996). Similarly, mutations in molecules associated with the laminin211 pathway, such as periaxin and frabin/FDG4, are responsible for Charcot-Marie-Tooth neuropathies (Sherman et al., 2001; Delague et al., 2007; Stendel et al., 2007). Thus, Jab1 may constitute a key molecule in the pathogenesis of some genetic neuropathies and together with p27 may become a valuable candidate target for therapies aimed at treating these genetic neuropathies.

MATERIALS AND METHODS

Mice. Mice carrying floxed *Jab1* alleles (*Jab1*$^{fl/fl}$, C57BL/6J background; Panattoni et al., 2008) were crossed with mP0TOTA (*P0-cre*, C57BL/6J) transgenic mice (Feltri et al., 1999) to specifically delete *Jab1* in Schwann cells. *Jab1*$^{fl/fl}$ *P0-cre* mice were maintained by backcrosses with C57BL/6J. Integrin β1 (*Itb1*$^{fl/fl}$; provided by U. Mueller, The Scripps Research Institute, La Jolla, CA), *dy3K* (laminin211$^{-/-}$; provided by S. Takeda, National Institute of Neuroscience, Tokyo, Japan), and *CRD*$^{+/-}$ (Nrg1 type III$^{+/-}$; provided by C. Taveggia, San Raffaele Scientific Institute, Milan, Italy) mice were previously described and all maintained in the C57BL/6J background (Miyagoe et al., 1997; Wolpowitz et al., 2000; Feltri et al., 2002). *p27*$^{-/-}$ (B6.129S$_4$-cdkn1b^{tm1Mlf}/J, strain C57BL/6J) and *dy2J* (C57BL/6J-Lama2^{dy-2J}) mice were purchased from the Jackson Laboratory. The transgenic mouse carrying the Mpz Ser63del mutation was in the FVB/N background strain and previously reported (Wrabetz et al., 2006). Fig4$^{-/-}$ (plt/plt) mice were provided by A. Bolino (San Raffaele Scientific Institute) and maintained on the recombinant inbred line CB.plt derived from strains CAST/Ei and C56BL/6J (25%) and previously described (Chow et al., 2007). For routine genotyping, we isolated genomic DNA from tail biopsies using DirectPCR solution (ViaGen), according to the manufacturer's directions. All animal experiments were approved and performed in compliance with the guidelines of San Raffaele Institutional Animal Care and Use Committee.

Rotarod analysis. 3-mo-old mice (13 *Jab1*$^{-/-}$ and 13 control littermates) were placed on a round metal bar rotating with acceleration from 4 to 40 rotations per minute (Ugo Basile). The mice were allowed to stay on the rod for a maximum of 900 s, and the time of hold on the rotating rod was measured in subsequent trials (one pretrial and two trials per day for three consecutive days).

Neurophysiology. Neurophysiology was performed as described previously (Triolo et al., 2006). We analyzed *Jab1*$^{-/-}$ versus WT mice (P60), *p27*$^{-/-}$ versus WT mice (P60), and *Jab1*$^{-/-}$ versus *Jab1*$^{-/-}$*p27*$^{-/-}$ and versus WT mice (P30). Mice were anesthetized with Avertin and placed under a heating lamp to avoid hypothermia. Sciatic NCVs were obtained by stimulating the nerve with steel monopolar needle electrodes. A pair of stimulating electrodes was inserted subcutaneously near the nerve at the ankle. A second pair of electrodes was placed at the sciatic notch to obtain two distinct sites of stimulation, proximal and distal, along the nerve. The muscular response to the electrical nerve stimulation (cMAPs) was recorded with a pair of needle electrodes; the active electrode was inserted in muscles in the middle of the paw, whereas the reference was placed in the skin between the first and second digit.

Histology and morphometric analysis. Semithin and ultrathin morphological experiments were performed as described previously (Wrabetz et al., 2000). In brief, sciatic nerves were removed and fixed with 2% (vol/vol) glutaraldehyde in 0.12 M phosphate buffer, postfixed with 1% (wt/vol) osmium tetroxide, and embedded in epon (Fluka). Semithin sections (0.5–1 µm thick) were stained with toluidine blue and examined by light microscopy (BX51; Olympus). Ultrathin sections (100–120 nm thick) were stained with uranyl acetate and lead citrate and examined by electron microscopy (CEM 902; Carl Zeiss). Digitalized images of fiber cross sections were obtained from corresponding levels of the sciatic nerve with a digital camera (DFC300F; Leica) using a 100× objective. At least five images from four different mice per genotype were acquired (30×10^3 µm^2 of sciatic nerve per each mouse). Morphometry on semithin sections was analyzed using ImageJ (National Institutes of Health) or QWin software (Leica; Triolo et al., 2006). The ratio between the mean diameter of an axon and the mean diameter of the fiber including myelin (g ratio) was determined on at least 500 randomly chosen fibers per mouse (five mice per genotype). To evaluate internodal length, glutaraldehyde-fixed sciatic nerves from P60 WT and *p27*$^{-/-}$ mice were osmicated and placed in glycerol. Single fibers were separated with fine forceps, placed on slides, and analyzed with a light microscope (BX51). Internodal length was measured on 100 teased nerve fibers per mouse (three mice per genotype). Schwann cell number was evaluated in longitudinal sections of sciatic nerves, counting the number of DAPI-positive nuclei in S100-positive cells (three mice per genotype per time point).

Primary cell cultures. Mouse and rat DRGs were isolated from E13.5 and E15.5 embryos, respectively, and plated on collagen-coated glass coverslips as described previously (Previtali et al., 2003; Taveggia et al., 2005). To establish rat Schwann cell/DRG co-cultures, DRGs were trypsinized (0.25%; Gibco) and mechanically dissociated. Cell suspension (approximately three DRGs) was plated as a drop onto 12-mm glass coverslips (Greiner) coated with 0.2 mg/ml rat collagen (Trevigen) in C-media, consisting of MEM (Gibco) supplemented with (final concentration) 10% FCS (Invitrogen), 4 mg/ml glucose (Sigma-Aldrich), 2 mM L-glutamine (Sigma-Aldrich), and 50 ng/ml nerve growth factor (NGF; Harlan or EMD Millipore). DRGs were then placed in neurobasal medium (NB; Gibco) supplemented with B27 (Gibco) and NGF as before until neuritogenesis was fully achieved. For myelination, DRGs were placed on C-media supplemented with 50 µg/ml ascorbic acid for 15 d (Sigma-Aldrich). To obtain purified rat neuronal cultures, explants prepared as above were treated with fluorodeoxyuridine (FdU; Sigma-Aldrich) plus

uridine (Sigma-Aldrich) to eliminate all nonneuronal cells. Primary rat Schwann cells were prepared as described previously (Previtali et al., 2003) and maintained in DMEM, 10% FBS, 2 mM L-glutamine (Invitrogen), 2 ng/ml recombinant human Nrg1-b1 (R&D Systems), and 2 mM forskolin (EMD Millipore) until used. To establish mouse Schwann cell/DRG co-culture explants, mouse DRGs were plated on collagen-coated coverslips (1:1). After 6 d of NB + B27, myelination was induced with C-media supplemented with ascorbic acid for 15 d.

Antibodies. Antibodies used for Western blot included (p, polyclonal; m, monoclonal; Ch, chicken; Ms, mouse; Rb, rabbit; Gt, goat; and Rt, rat) Jab1 (pRb; 1:1,000; Sigma-Aldrich), β-tubulin (mMs; 1:1,000; Sigma-Aldrich), laminin α2 (mMs; 1:200; clone 2D9; gift from H. Hori, Tokyo Medical and Dental University, Tokyo, Japan), calnexin (pRb; 1:5,000; Sigma-Aldrich), oct6 (pRb; 1:1,000; gift from D. Meijer, Erasmus University Medical Center, Rotterdam, Netherlands), krox20 (pRb; 1:600; Covance), c-Jun (pRb; 1:1,000; Cell Signaling Technology), p-cJun (pRb; 1:1,000; Cell Signaling Technology), cyclin A (pRb; 1:200; Santa Cruz Biotechnology, Inc.), cyclin B1 (pGt; 1:10,000; R&D Systems), cyclin D1 (pRb; 1:1,000; EMD Millipore), cyclin E (pRb; 1:1,000; EMD Millipore), $p27^{Kip1}$ (mMs; 1:1,000; BD), p21 (mMs; 1:200; BD), gapdh (mMs; 1:500; EMD Millipore), ErbB2 (pRb; 1:200; Santa Cruz Biotechnology, Inc.), and p-ErbB2 (pRb; 1:50; Santa Cruz Biotechnology, Inc.). Secondary antibodies were as follows: anti–rabbit (1:10,000; Sigma-Aldrich) and anti–mouse (1:10,000; eBioscience) conjugated with horseradish peroxidase and anti–rabbit (1:10,000; IRDye680; LI-COR Biosciences) and anti–mouse (1:10,000; IRDye800CW; LI-COR Biosciences) conjugated with fluorochrome. Antibodies used for immunohistochemistry included mbp (mRt; 1:50; EMD Millipore), neurofilament M (pCh; 1:1,000; Covance), BrdU (mMs; 1:20; Roche), Ki67 (pRb; 1:100; NCL-Ki67p; Novocastra), laminin α2 (mRt; 1:100; clone 4H8-2; Alexis), oct6 (pRb; 1:200; gift from D. Meijer), and krox20 (pRb; 1:800; Covance). Secondary antibodies for detection of rabbit, mouse, or rat antibodies were used conjugated with fluorochromes FITC or TRIC (Jackson ImmunoResearch Laboratories, Inc.). Slide mounting medium was used with DAPI (H-1200;Vectashield).

Immunohistochemistry. Immunofluorescence on cryosections was performed as described previously (Triolo et al., 2006) and examined with confocal (SP5; Leica) and fluorescent microscope (BX51). For teased fiber preparation, sciatic nerves were removed and fixed on ice in freshly prepared buffered 4% paraformaldehyde, as described previously (Bolino et al., 2004). Single fibers were separated with fine forceps and placed on slides. Slides with teased fibers were immersed in cold acetone for 5 min, rehydrated with TBS, and then blocked at room temperature for 1 h in 5% fish skin gelatin, containing 0.5% Triton X-100 in PBS. Slides were incubated over night at 4°C with primary antibodies diluted in blocking solution. After incubation, the slides were washed in TBS and incubated with appropriate secondary antibodies and mounted with Vectashield (Vector Laboratories).

BrdU and TUNEL assays. Schwann cell proliferation was evaluated in vivo in sciatic nerves by BrdU incorporation (Roche) and BrdU/Ki67 double immunolabeling as previously described (Feltri et al., 2002). In brief, timed pregnant females (E17.5) or individual mice (P5 and P30) were injected intraperitoneally with BrdU (100 µg/g body weight), and animals were killed by decapitation 1 h later. 7-µm cryosections of the posterior limbs from fetuses or sciatic nerve of mutant or control mice were fixed in cold methanol, treated with 2N HCl for 15 min at 37°C, and neutralized with 0.1 M sodium borate, pH 8.5, for 10 min. Slides were then incubated overnight with pAb anti-Ki67 and successively with pAb anti–neurofilament M and mAb anti-BrdU to identify nerves and proliferating cells, respectively. After staining with secondary antibodies, nuclei were counterstained with DAPI (Vectashield). Only cigar-shaped nuclei associated with nerves were counted, and the fraction of BrdU- and Ki67-positive nuclei was determined. At least 3,500 nuclei at E17.5 and 10,000 nuclei at P5 and P30 were examined. Apoptotic cells were detected in sciatic nerves by terminal deoxynucleotidyl transferase (TdT)–mediated dUTP-biotin nick end labeling (TUNEL) as described previously (Feltri et al., 2002). For quantification, DAPI-positive nuclei associated with nerves (NF-M positive) were counted, and the fraction of TUNEL-positive nuclei was determined. At least 3,500 at E17.5 and 10,000 nuclei at P1, P5, P15, and P60 were examined.

Western blot. Proteins were isolated from snap-frozen sciatic nerves of mice, and Western blotting was performed as described previously (Triolo et al., 2006). In brief, nerves were homogenized in lysis buffer containing 1% (vol/vol) Triton, 20 mM Tris-HCl, pH 7.5, 150 mM NaCl, 10 mM $MgCl_2$, phosphatase inhibitor (PhoSTOP; Roche), and protease inhibitors (Complete-Mini EDTA free; Roche). Homogenates were sonicated and centrifuged for 10 min at 12,000 rpm at 4°C. Protein concentrations were determined by BCA method (Bio-Rad Laboratories). Equal amounts of homogenates (150 µg for cyclin B1, 50 µg for erbB2, and 10–20 µg for other proteins) were fractionated by SDS-PAGE and blotted onto PVDF (EMD Millipore) or nitrocellulose (Bio-Rad Laboratories). Membranes were blocked in 5% no-fat dry milk in TBST (0.1% Triton X-100 in TBS) incubated with specific primary and secondary antibodies, washed in TBST, and developed with the ECL chemiluminescent substrate (GE Healthcare) or analyzed using the Odyssey Infrared Imaging System (LI-COR Biosciences) according to the manufacturer's instructions.

Semiquantitative and quantitative RT-PCR. Total RNA was isolated from Schwann cells, DRG neurons, and nerves using TriPure Isolation Reagent (Roche) according to the manufacturer's instructions. In brief, cells or nerves were homogenized in the presence of TriPure Isolation Reagent, and total RNA was extracted with chloroform and precipitated with isopropanol. A portion (100 ng) of total RNA was reverse transcribed using a High-Capacity cDNA Reverse Transcription kit (Applied Biosystems). Semiquantitative RT-PCR analyses were performed using a primer pair for *Jab1* and *Gapdh*. Quantitative RT-PCR analyses were performed on a 7900HT Real-Time PCR System using the 2× TaqMan PCR Mastermix (Applied Biosystems) according to manufacturer's recommendations. The primers used were TaqMan Gene Expression Assays ID Mm00489065_m1 for *Cops5/Jab1* and Mm99999915_g1 for *Gapdh*. Levels of gene expression were determined with the comparative cycle threshold ($\Delta\Delta C_t$) method. The mRNA level of *Jab1* gene was normalized to the level of *Gapdh* mRNA. Each time point is the mean of five experiments (each experiment was performed with a pool of five to seven nerves).

Statistical analysis. Data are presented as means ± SEM. Statistical analyses were evaluated by paired or unpaired two-tailed Student's *t* test in all of the experiments. Statistical differences were considered to be significant for $P \le 0.05$ (*, $P \le 0.05$; **, $P \le 0.01$; ***, $P \le 0.001$). All statistical analyses were performed using Instat software (GraphPad Software).

Online supplemental material. Video 1 shows the phenotype of a *Jab1*$^{-/-}$ mouse (5 mo old) as compared with an age-matched WT mouse. Online supplemental material is available at http://www.jem.org/cgi/content/full/jem.20130720/DC1.

We are grateful to Carla Taveggia and Alessandra Bolino for critical reading and suggestions and Paola Podini for the help with and Alembic for the use of the electron microscope.

This work was supported by grants from the Telethon Italy Foundation (GGP08037, GPP10007, and GGP12024 to S.C. Previtali), FISM (2011/R/30 to S.C. Previtali), and National Institutes of Health (R01NS NS045630 to M.L. Feltri).

The authors have no conflicting financial interests.

Submitted: 7 April 2013
Accepted: 25 November 2013

REFERENCES

Atanasoski, S., D. Boller, L. De Ventura, H. Koegel, M. Boentert, P. Young, S. Werner, and U. Suter. 2006. Cell cycle inhibitors p21 and p16 are required for the regulation of Schwann cell proliferation. *Glia*. 53:147–157. http://dx.doi.org/10.1002/glia.20263

Bardin, A.J., and A. Amon. 2001. Men and sin: what's the difference? *Nat. Rev. Mol. Cell Biol.* 2:815–826. http://dx.doi.org/10.1038/35099020

Benninger, Y., T. Thurnherr, J.A. Pereira, S. Krause, X. Wu, A. Chrostek-Grashoff, D. Herzog, K.A. Nave, R.J. Franklin, D. Meijer, et al. 2007. Essential and distinct roles for cdc42 and rac1 in the regulation of Schwann cell biology during peripheral nervous system development. *J. Cell Biol.* 177:1051–1061. http://dx.doi.org/10.1083/jcb.200610108

Berti, C., L. Bartesaghi, M. Ghidinelli, D. Zambroni, G. Figlia, Z.L. Chen, A. Quattrini, L. Wrabetz, and M.L. Feltri. 2011. Non-redundant function of dystroglycan and β1 integrins in radial sorting of axons. *Development.* 138:4025–4037. http://dx.doi.org/10.1242/dev.065490

Birchmeier, C., and K.A. Nave. 2008. Neuregulin-1, a key axonal signal that drives Schwann cell growth and differentiation. *Glia.* 56:1491–1497. http://dx.doi.org/10.1002/glia.20753

Bolino, A., A. Bolis, S.C. Previtali, G. Dina, S. Bussini, G. Dati, S. Amadio, U. Del Carro, D.D. Mruk, M.L. Feltri, et al. 2004. Disruption of Mtmr2 produces CMT4B1-like neuropathy with myelin outfolding and impaired spermatogenesis. *J. Cell Biol.* 167:711–721. http://dx.doi.org/10.1083/jcb.200407010

Bradley, W.G., and M. Jenkison. 1973. Abnormalities of peripheral nerves in murine muscular dystrophy. *J. Neurol. Sci.* 18:227–247. http://dx.doi.org/10.1016/0022-510X(73)90009-9

Bray, G.M., S. David, T. Carlstedt, and A.J. Aguayo. 1983. Effects of crush injury on the abnormalities in the spinal roots and peripheral nerves of dystrophic mice. *Muscle Nerve.* 6:497–503. http://dx.doi.org/10.1002/mus.880060705

Casaccia-Bonnefil, P., R.J. Hardy, K.K. Teng, J.M. Levine, A. Koff, and M.V. Chao. 1999. Loss of p27Kip1 function results in increased proliferative capacity of oligodendrocyte progenitors but unaltered timing of differentiation. *Development.* 126:4027–4037.

Chamovitz, D.A., and D. Segal. 2001. JAB1/CSN5 and the COP9 signalosome. A complex situation. *EMBO Rep.* 2:96–101. http://www.nature.com/embor/journal/v2/n2/full/embor480.html

Chen, Z.L., and S. Strickland. 2003. Laminin γ1 is critical for Schwann cell differentiation, axon myelination, and regeneration in the peripheral nerve. *J. Cell Biol.* 163:889–899. http://dx.doi.org/10.1083/jcb.200307068

Cheng, X., Z. Zhou, G. Xu, J. Zhao, H. Wu, L. Long, H. Wen, X. Gu, and Y. Wang. 2013. Dynamic changes of Jab1 and p27kip1 expression in injured rat sciatic nerve. *J. Mol. Neurosci.* 51:148–158. http://dx.doi.org/10.1007/s12031-013-9969-8

Chow, C.Y., Y. Zhang, J.J. Dowling, N. Jin, M. Adamska, K. Shiga, K. Szigeti, M.E. Shy, J. Li, X. Zhang, et al. 2007. Mutation of FIG4 causes neurodegeneration in the pale tremor mouse and patients with CMT4J. *Nature.* 448:68–72. http://dx.doi.org/10.1038/nature05876

Delague, V., A. Jacquier, T. Hamadouche, Y. Poitelon, C. Baudot, I. Boccaccio, E. Chouery, M. Chaouch, N. Kassouri, R. Jabbour, et al. 2007. Mutations in FGD4 encoding the Rho GDP/GTP exchange factor FRABIN cause autosomal recessive Charcot-Marie-Tooth type 4H. *Am. J. Hum. Genet.* 81:1–16. http://dx.doi.org/10.1086/518428

Feltri, M.L., and L. Wrabetz. 2005. Laminins and their receptors in Schwann cells and hereditary neuropathies. *J. Peripher. Nerv. Syst.* 10:128–143. http://dx.doi.org/10.1111/j.1085-9489.2005.0010204.x

Feltri, M.L., M. D'antonio, A. Quattrini, R. Numerato, M. Arona, S. Previtali, S.Y. Chiu, A. Messing, and L. Wrabetz. 1999. A novel P0 glycoprotein transgene activates expression of lacZ in myelin-forming Schwann cells. *Eur. J. Neurosci.* 11:1577–1586. http://dx.doi.org/10.1046/j.1460-9568.1999.00568.x

Feltri, M.L., D. Graus Porta, S.C. Previtali, A. Nodari, B. Migliavacca, A. Cassetti, A. Littlewood-Evans, L.F. Reichardt, A. Messing, A. Quattrini, et al. 2002. Conditional disruption of beta 1 integrin in Schwann cells impedes interactions with axons. *J. Cell Biol.* 156:199–209. http://dx.doi.org/10.1083/jcb.200109021

Grove, M., N.H. Komiyama, K.A. Nave, S.G. Grant, D.L. Sherman, and P.J. Brophy. 2007. FAK is required for axonal sorting by Schwann cells. *J. Cell Biol.* 176:277–282. http://dx.doi.org/10.1083/jcb.200609021

Guo, L.T., X.U. Zhang, W. Kuang, H. Xu, L.A. Liu, J.T. Vilquin, Y. Miyagoe-Suzuki, S. Takeda, M.A. Ruegg, U.M. Wewer, and E. Engvall. 2003. Laminin alpha2 deficiency and muscular dystrophy; genotype-phenotype correlation in mutant mice. *Neuromuscul. Disord.* 13:207–215. http://dx.doi.org/10.1016/s0960-8966(02)00266-3

Henry, M.D., J.S. Satz, C. Brakebusch, M. Costell, E. Gustafsson, R. Fässler, and K.P. Campbell. 2001. Distinct roles for dystroglycan, β1 integrin and perlecan in cell surface laminin organization. *J. Cell Sci.* 114:1137–1144.

Hsu, M.C., H.C. Chang, and W.C. Hung. 2007. HER-2/neu transcriptionally activates Jab1 expression via the AKT/beta-catenin pathway in breast cancer cells. *Endocr. Relat. Cancer.* 14:655–667. http://dx.doi.org/10.1677/ERC-07-0077

Jessen, K.R., and R. Mirsky. 2005. The origin and development of glial cells in peripheral nerves. *Nat. Rev. Neurosci.* 6:671–682. http://dx.doi.org/10.1038/nrn1746

Larrea, M.D., S.A. Wander, and J.M. Slingerland. 2009. p27 as Jekyll and Hyde: regulation of cell cycle and cell motility. *Cell Cycle.* 8:3455–3461. http://dx.doi.org/10.4161/cc.8.21.9789

Levinson, H., A.K. Sil, J.E. Conwell, J.E. Hopper, and H.P. Ehrlich. 2004. Alpha V integrin prolongs collagenase production through Jun activation binding protein 1. *Ann. Plast. Surg.* 53:155–161. http://dx.doi.org/10.1097/01.sap.0000112281.97409.a6

Li, H., H. Yang, Y. Liu, W. Huan, S. Zhang, G. Wu, Q. Lu, Q. Wang, and Y. Wang. 2011. The cyclin-dependent kinase inhibitor p27(Kip1) is a positive regulator of Schwann cell differentiation in vitro. *J. Mol. Neurosci.* 45:277–283. http://dx.doi.org/10.1007/s12031-011-9518-2

Martin, J.R., and H.D. Webster. 1973. Mitotic Schwann cells in developing nerve: their changes in shape, fine structure, and axon relationships. *Dev. Biol.* 32:417–431. http://dx.doi.org/10.1016/0012-1606(73)90251-0

Mercuri, E., J. Pennock, F. Goodwin, C. Sewry, F. Cowan, L. Dubowitz, V. Dubowitz, and F. Muntoni. 1996. Sequential study of central and peripheral nervous system involvement in an infant with merosin-deficient congenital muscular dystrophy. *Neuromuscul. Disord.* 6:425–429. http://dx.doi.org/10.1016/S0960-8966(96)00383-5

Miyagoe, Y., K. Hanaoka, I. Nonaka, M. Hayasaka, Y. Nabeshima, K. Arahata, Y. Nabeshima, and S. Takeda. 1997. Laminin alpha2 chain-null mutant mice by targeted disruption of the Lama2 gene: a new model of merosin (laminin 2)-deficient congenital muscular dystrophy. *FEBS Lett.* 415:33–39. http://dx.doi.org/10.1016/S0014-5793(97)01007-7

Nakagawa, M., Y. Miyagoe-Suzuki, K. Ikezoe, Y. Miyata, I. Nonaka, K. Harii, and S. Takeda. 2001. Schwann cell myelination occurred without basal lamina formation in laminin α2 chain-null mutant (dy^{3K}/dy^{3K}) mice. *Glia.* 35:101–110. http://dx.doi.org/10.1002/glia.1075

Nave, K.A., and J.L. Salzer. 2006. Axonal regulation of myelination by neuregulin 1. *Curr. Opin. Neurobiol.* 16:492–500. http://dx.doi.org/10.1016/j.conb.2006.08.008

Nodari, A., D. Zambroni, A. Quattrini, F.A. Court, A. D'Urso, A. Recchia, V.L. Tybulewicz, L. Wrabetz, and M.L. Feltri. 2007. Beta1 integrin activates Rac1 in Schwann cells to generate radial lamellae during axonal sorting and myelination. *J. Cell Biol.* 177:1063–1075. http://dx.doi.org/10.1083/jcb.200610014

Panattoni, M., F. Sanvito, V. Basso, C. Doglioni, G. Casorati, E. Montini, J.R. Bender, A. Mondino, and R. Pardi. 2008. Targeted inactivation of the COP9 signalosome impairs multiple stages of T cell development. *J. Exp. Med.* 205:465–477. http://dx.doi.org/10.1084/jem.20070725

Pereira, J.A., Y. Benninger, R. Baumann, A.F. Gonçalves, M. Ozçelik, T. Thurnherr, N. Tricaud, D. Meijer, R. Fässler, U. Suter, and J.B. Relvas. 2009. Integrin-linked kinase is required for radial sorting of axons and Schwann cell remyelination in the peripheral nervous system. *J. Cell Biol.* 185:147–161. http://dx.doi.org/10.1083/jcb.200809008

Previtali, S.C., A. Nodari, C. Taveggia, C. Pardini, G. Dina, A. Villa, L. Wrabetz, A. Quattrini, and M.L. Feltri. 2003. Expression of laminin receptors in schwann cell differentiation: evidence for distinct roles. *J. Neurosci.* 23:5520–5530.

Raphael, A.R., D.A. Lyons, and W.S. Talbot. 2011. ErbB signaling has a role in radial sorting independent of Schwann cell number. *Glia.* 59:1047–1055. http://dx.doi.org/10.1002/glia.21175

Shackleford, T.J., and F.X. Claret. 2010. JAB1/CSN5: a new player in cell cycle control and cancer. *Cell Div.* 5:26. http://dx.doi.org/10.1186/1747-1028-5-26

Sherman, D.L., and P.J. Brophy. 2005. Mechanisms of axon ensheathment and myelin growth. *Nat. Rev. Neurosci.* 6:683–690. http://dx.doi.org/10.1038/nrn1743

Sherman, D.L., C. Fabrizi, C.S. Gillespie, and P.J. Brophy. 2001. Specific disruption of a schwann cell dystrophin-related protein complex in a demyelinating neuropathy. *Neuron.* 30:677–687. http://dx.doi.org/10.1016/S0896-6273(01)00327-0

Shorer, Z., J. Philpot, F. Muntoni, C. Sewry, and V. Dubowitz. 1995. Demyelinating peripheral neuropathy in merosin-deficient congenital

muscular dystrophy. *J. Child Neurol.* 10:472–475. http://dx.doi.org/10.1177/088307389501000610

Stendel, C., A. Roos, T. Deconinck, J. Pereira, F. Castagner, A. Niemann, J. Kirschner, R. Korinthenberg, U.P. Ketelsen, E. Battaloglu, et al. 2007. Peripheral nerve demyelination caused by a mutant Rho GTPase guanine nucleotide exchange factor, frabin/FGD4. *Am. J. Hum. Genet.* 81:158–164. http://dx.doi.org/10.1086/518770

Stevens, B., and R.D. Fields. 2002. Regulation of the cell cycle in normal and pathological glia. *Neuroscientist.* 8:93–97. http://dx.doi.org/10.1177/107385840200800205

Stirling, C.A. 1975. Abnormalities in Schwann cell sheaths in spinal nerve roots of dystrophic mice. *J. Anat.* 119:169–180.

Taveggia, C., G. Zanazzi, A. Petrylak, H. Yano, J. Rosenbluth, S. Einheber, X. Xu, R.M. Esper, J.A. Loeb, P. Shrager, et al. 2005. Neuregulin-1 type III determines the ensheathment fate of axons. *Neuron.* 47:681–694. http://dx.doi.org/10.1016/j.neuron.2005.08.017

Tomoda, K., Y. Kubota, Y. Arata, S. Mori, M. Maeda, T. Tanaka, M. Yoshida, N. Yoneda-Kato, and J.Y. Kato. 2002. The cytoplasmic shuttling and subsequent degradation of p27Kip1 mediated by Jab1/CSN5 and the COP9 signalosome complex. *J. Biol. Chem.* 277:2302–2310. http://dx.doi.org/10.1074/jbc.M104431200

Triolo, D., G. Dina, I. Lorenzetti, M. Malaguti, P. Morana, U. Del Carro, G. Comi, A. Messing, A. Quattrini, and S.C. Previtali. 2006. Loss of glial fibrillary acidic protein (GFAP) impairs Schwann cell proliferation and delays nerve regeneration after damage. *J. Cell Sci.* 119:3981–3993. http://dx.doi.org/10.1242/jcs.03168

Wang, D., F. He, L. Zhang, F. Zhang, Q. Wang, X. Qian, X. Pan, J. Meng, C. Peng, A. Shen, and J. Chen. 2011. The role of p27(Kip1) phosphorylation at serine 10 in the migration of malignant glioma cells in vitro. *Neoplasma.* 58:65–73.

Webster, H.D. 1993. Development of peripheral nerve fibers. *In* Peripheral Neuropathy. Vol. I. P. Dyck, P. Thomas, J. Griffin, P. Low, and J. Poduslo, editors. Saunders Co., Philadelphia. 243–266.

Webster, H.D., R. Martin, and M.F. O'Connell. 1973. The relationships between interphase Schwann cells and axons before myelination: a quantitative electron microscopic study. *Dev. Biol.* 32:401–416. http://dx.doi.org/10.1016/0012-1606(73)90250-9

Wei, Q., W.K. Miskimins, and R. Miskimins. 2003. The Sp1 family of transcription factors is involved in p27(Kip1)-mediated activation of myelin basic protein gene expression. *Mol. Cell. Biol.* 23:4035–4045. http://dx.doi.org/10.1128/MCB.23.12.4035-4045.2003

Wolpowitz, D., T.B. Mason, P. Dietrich, M. Mendelsohn, D.A. Talmage, and L.W. Role. 2000. Cysteine-rich domain isoforms of the neuregulin-1 gene are required for maintenance of peripheral synapses. *Neuron.* 25:79–91. http://dx.doi.org/10.1016/S0896-6273(00)80873-9

Wrabetz, L., M.L. Feltri, A. Quattrini, D. Imperiale, S. Previtali, M. D'Antonio, R. Martini, X. Yin, B.D. Trapp, L. Zhou, et al. 2000. P_0 glycoprotein overexpression causes congenital hypomyelination of peripheral nerves. *J. Cell Biol.* 148:1021–1034. http://dx.doi.org/10.1083/jcb.148.5.1021

Wrabetz, L., M. D'Antonio, M. Pennuto, G. Dati, E. Tinelli, P. Fratta, S. Previtali, D. Imperiale, J. Zielasek, K. Toyka, et al. 2006. Different intracellular pathomechanisms produce diverse Myelin Protein Zero neuropathies in transgenic mice. *J. Neurosci.* 26:2358–2368. http://dx.doi.org/10.1523/JNEUROSCI.3819-05.2006

Xu, H., X.-R. Wu, U.M. Wewer, and E. Engvall. 1994. Murine muscular dystrophy caused by a mutation in the laminin alpha 2 (Lama2) gene. *Nat. Genet.* 8:297–302. http://dx.doi.org/10.1038/ng1194-297

Yang, D., J. Bierman, Y.S. Tarumi, Y.P. Zhong, R. Rangwala, T.M. Proctor, Y. Miyagoe-Suzuki, S. Takeda, J.H. Miner, L.S. Sherman, et al. 2005. Coordinate control of axon defasciculation and myelination by laminin-2 and -8. *J. Cell Biol.* 168:655–666. http://dx.doi.org/10.1083/jcb.200411158

Yu, W.M., M.L. Feltri, L. Wrabetz, S. Strickland, and Z.L. Chen. 2005. Schwann cell-specific ablation of laminin gamma1 causes apoptosis and prevents proliferation. *J. Neurosci.* 25:4463–4472. http://dx.doi.org/10.1523/JNEUROSCI.5032-04.2005